Nanoscale Advances

ROYAL SOCIETY OF CHEMISTRY

PAPER

View Article Online
View Journal | View Issue

Cite this: *Nanoscale Adv.*, 2021, **3**, 3835

Selective area growth of GaN nanowires and nanofins by molecular beam epitaxy on heteroepitaxial diamond (001) substrates†

Florian Pantle, * Fabian Becker, Max Kraut, Simon Wörle, Theresa Hoffmann, Sabrina Artmeier and Martin Stutzmann *

GaN-on-diamond is a promising route towards reliable high-power transistor devices with outstanding performances due to better heat management, replacing common GaN-on-SiC technologies. Nevertheless, the implementation of GaN-on-diamond remains challenging. In this work, the selective area growth of GaN nanostructures on cost-efficient, large-scale available heteroepitaxial diamond (001) substrates by means of plasma-assisted molecular beam epitaxy is investigated. Additionally, we discuss the influence of an AlN buffer on the morphology of the GaN nanostructures. The nanowires and nanofins are characterized by a very high selectivity and controllable dimensions. Low temperature photoluminescence measurements are used to evaluate their structural quality. The growth of two GaN crystal domains, which are in-plane rotated against each other by 30°, is observed. The favoring of a certain domain is determined by the off-cut direction of the diamond substrates. By X-ray diffraction we show that the GaN nanostructures grow perpendicular to the diamond surface on off-cut diamond (001) substrates, which is in contrast to the growth on diamond (111), where the nanostructures are aligned with the substrate lattice. Polarity-selective wet chemical etching and Kelvin probe force microscopy reveal that the GaN nanostructures grow solely in the Ga-polar direction. This is a major advantage compared to the growth on diamond (111) and enables the application of GaN nanostructures on cost-efficient diamond for high-power/high-frequency applications.

Received 23rd March 2021
Accepted 4th May 2021

DOI: 10.1039/d1na00221j

rsc.li/nanoscale-advances

Introduction

Group III-nitride nanorods/nanowires (NWs) and nanowalls/nanofins (NFs) are expected to be applied in photo-catalysis,[1–3] sensing devices,[4–7] optoelectronics,[8–14] and high-power electronics.[15–20] In particular, selectively grown GaN nanostructures (NSs) benefit from outstanding structural quality, *e.g.*, due to strain relaxation and dislocation filtering,[21–24] making them a promising candidate for next-generation three-dimensional GaN-based NW/NF field-effect transistors (NWFETs/FinFETs). Nevertheless, GaN-based high-electron-mobility transistors (HEMTs) suffer from self-heating during high-frequency and high-voltage operation leading to device damage. A promising route towards reliable and high-performance devices is the integration of GaN-based HEMTs on diamond enabling efficient heat dissipation through the substrate due to the unique thermal conductivity of diamond.[25–27] GaN NSs selectively grown on diamond introduce a promising path towards future devices, which combine the high crystal quality of GaN NSs with the beneficial 3D device design on a highly efficient heat-dissipating substrate. In contrast to the established selective area growth (SAG) of wurtzite GaN NSs on (quasi-)hexagonal single crystalline diamond (SCD) (111), the growth on the cubic (001) surface of diamond is more challenging, especially when using technologically relevant heteroepitaxially grown diamond (HD) substrates.

Here, we present the optimization of SAG of GaN NSs by plasma-assisted molecular beam epitaxy (MBE) on cost-efficient, large-scale available HD (001) with and without AlN buffer layers. X-ray diffraction (XRD) measurements of the group III-nitride/diamond heterojunctions were used to determine their epitaxial relationship, while low temperature photoluminescence (PL) measurements were conducted to analyze the structural quality of the GaN NSs. In addition, by selective wet-chemical etching and Kelvin probe force microscopy (KPFM) of the GaN NSs, information about their polarity was obtained. As a result, we demonstrate high quality SAG of unipolar GaN NSs on scalable HD (001), which offers a unique advantage for their application in high-power electronics.

Walter Schottky Institut and Physics Department, Technische Universität München, Am Coulombwall 4, 85748 Garching, Germany. E-mail: florian.pantle@wsi.tum.de; stutz@wsi.tum.de

† Electronic supplementary information (ESI) available: High resolution XRD measurements and AFM images of the diamond substrates, X-ray reflectivity measurements of the AlN buffer layer on HD (001), and SEM images of non-coalescent GaN NFs at the lithographic limits, and GaN NSs on AlN-buffered and bare HD (001) before and after polarity-selective etching. See DOI: 10.1039/d1na00221j

Results and discussion

AlN buffer

In order to investigate the influence of an AlN buffer layer on the epitaxy of GaN NSs on HD (001), an AlN layer was grown *via* MBE for 3 min, resulting in a layer thickness of 17 nm. This value was determined by X-ray reflectivity measurements assuming a native surface oxide on top of the buffer (14 nm AlN + 3 nm Al_xO_y). The corresponding data are shown in the ESI.† Such thin AlN films are favorable in order not to lose the beneficial properties of the substrate like the high thermal conductivity of diamond. Fig. 1a shows a 5 × 5 μm^2 atomic force microscopy (AFM) image of this AlN/HD (001) heterostructure showing a root mean square (RMS) roughness of 1.43 nm. Similar RMS roughnesses are reported in the literature for thicker (approx. 500 nm) AlN layers grown by MBE, metal–organic chemical vapor deposition and sputter deposition.[28–30] The surface morphology is dominated by the polishing grooves of the HD (001), which are parallel to [110]diamond (*cf.* Fig. S1b, ESI†). An image magnified to an area of 500 × 500 nm^2 is shown in Fig. 1b. It shows that the AlN buffer consists of small AlN crystallites homogeneously covering the whole diamond surface. The grainy layer consists of columns with an average diameter of (20 ± 10) nm.

Morphology of GaN NSs on diamond

Scanning electron microscopy (SEM) images of GaN NSs grown under optimized growth conditions on SCD (111), and bare and AlN-buffered HD (001) are shown in Fig. 2. On SCD (111) (Fig. 2a) the NWs have uniform dimensions and show the same morphology as reported earlier for this substrate.[31–33] The NWs are all slightly tilted by approx. 6° in the same direction. The GaN NFs on SCD (111) have smooth non-polar sidewalls and a comparably flat *c*-plane top facet. Note that the NWs and NFs are tilted in the same direction but only the perspective of view has been changed. The viewpoint of the NWs is chosen to highlight the tilt of the NWs while the NFs are imaged from a different direction to show their *m*-plane facets. Similarly to NFs on sapphire,[34] the in-plane crystal orientation of the NFs relative to SCD (111) is fixed due to the strong epitaxial relationship of $[10\bar{1}0]$GaN‖$[01\bar{1}]$diamond.[35]

GaN NWs on HD (001) (Fig. 2b) show single semi-polar top facets and homogeneous diameters with some sporadic outgrowths. These outgrowths, which might be triggered by multiple nucleation and undesirable coalescence of GaN crystal-seeds, are noticeable in the NFs as distortions of the otherwise smooth NF side walls. The top facets of the NFs are mostly flat (*c*-plane) but show more irregularities compared to

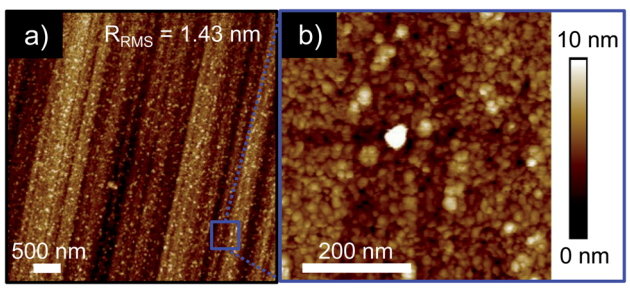

Fig. 1 (a) 5 × 5 μm^2 and (b) 500 × 500 nm^2 AFM images of the AlN buffer layer on HD (001).

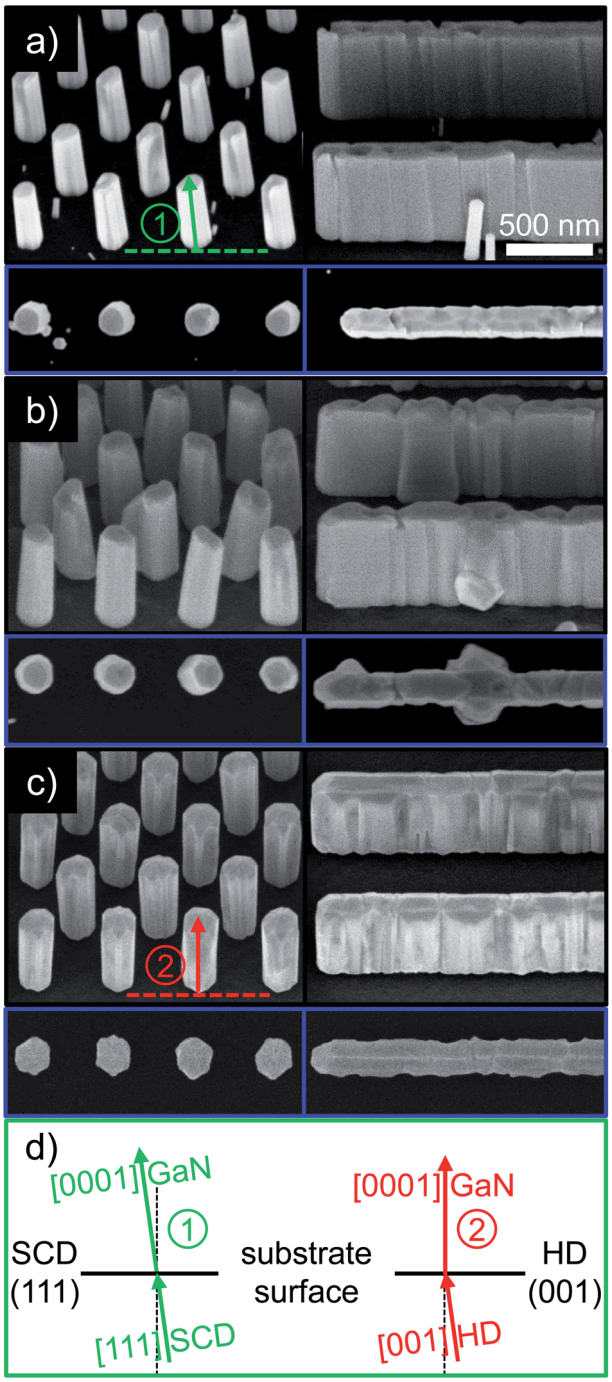

Fig. 2 SEM images with a 45°-tilted view (black-framed) and top view (blue-framed) of GaN NWs and NFs on (a) SCD (111), (b) HD (001), and (c) the AlN buffer layer on HD (001). (d) Schematic drawing of the GaN NS epitaxy on SCD (111) (green) and on HD (001) (red). The arrows indicate the lattice directions and the black lines represent the 5° off-cut diamond surfaces.

the NFs grown on SCD (111). Some of the NWs are tilted, but they do not have a preferred tilt direction. The NFs on HD (001) do not show a visible tilt.

GaN NWs grown on AlN-buffered HD (001) (Fig. 2c) have the most uniform appearance in terms of NW diameter, height and shape. While the NWs on both bare diamond substrates have mostly smooth, single-plane top facets pointing in different directions, the semi-polar top facets of the NWs on the AlN buffer taper towards one point above the middle of the wire with an angle of approx. 35° (*cf.* Fig. 6c). A similar morphology is observed for homoepitaxial GaN NWs grown on Ga-polar GaN templates. The almost hexagonal footprint with blunt edges of the NWs indicates that they are in a transition during the growth process from a dodecagonal shape with *m*- and *a*-plane side walls to their final, purely *m*-plane hexagonal shape with a pyramidal NW top.[36–39] Compared to the NWs on the bare (111) and (001) diamond substrates, the NWs grown on an AlN buffer seem to be in a later state of this transition as they already show more defined *m*-plane side facets. This might be due to the more designated epitaxy of GaN on AlN as both have the wurtzite crystal structure. On the cubic diamond surfaces, the hexagonal formation of the NWs seems to be delayed or a complete formation might not even take place. This could also explain the different NW top facets as the tapered NW top evolves during the last phase of the hexagonal side facet formation due to minimization of surface energy. In contrast, NW tops are more flat in earlier facet formation states.[38] A future nucleation study and an investigation of the influence of the growth duration on the NW morphology might help to better understand the growth kinetics. The NFs on AlN-buffered HD (001) have a uniform thickness with slightly ribbed side walls and semi-polar top facets. Neither the NWs nor the NFs show any tilt with respect to the substrate surface when grown on an AlN buffer. The SEM images indicate that the GaN NSs on SCD (111) grow in alignment with the diamond lattice and, thus, are tilted by approximately the off-cut angle as depicted in Fig. 2d. The NSs on HD (001), whether with or without AlN buffer, grow rather perpendicular to the polished diamond surface, which will be discussed in more detail in the XRD section below.

By changing the hole diameter (slit width) of the nano-patterns in the Ti mask, the NW (NF) thicknesses can be tuned. GaN NSs grown on AlN-buffered HD (001) with varying widths are shown in Fig. 3. The diameter of the GaN NWs can be tuned from approx. 210 nm up to 290 nm. The width of the NFs can be varied from 215 nm to 270 nm, which is a smaller range than reported for GaN NFs on sapphire (175 nm to 300 nm).[34] At smaller nominal fin widths, the NF is not continuous (Fig. S4a, ESI†). The lower limit of the NF thickness is not limited by MBE, but by the e-beam lithography process, as for the smallest doses minimal fluctuations of the e-beam current lead to residual undeveloped resist. This hinders a complete and undisturbed etching of the mask and consequently leads to non-regular nucleation. Further optimization of the lithography process might push the limit towards even thinner NFs. Nominal thicker fins result in a split-up of one NF into a "double/hollow fin" with no nucleation in the middle of the nano-slit itself due to an overexposure of the electron beam resist (Fig. S4b, ESI†) as thicker nano-slits have been gained by a higher dose of the line-exposure. A change in the e-beam procedure from a line- to an area-exposure might help to overcome this issue.

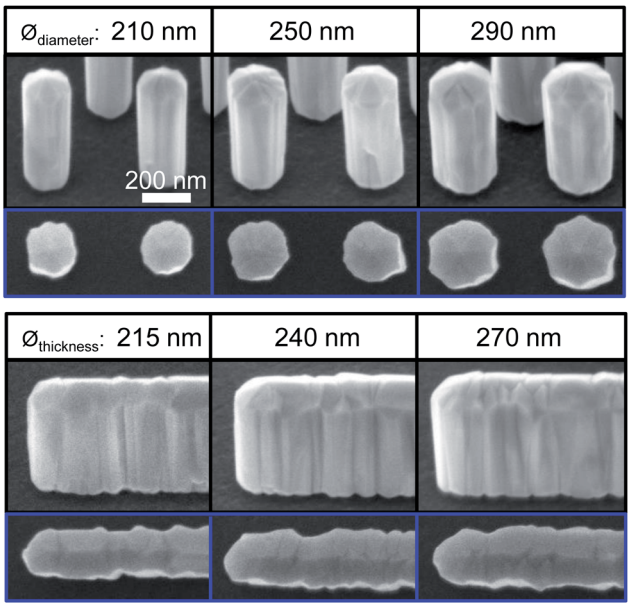

Fig. 3 SEM images of GaN NWs and NFs with varying diameter/thickness on AlN-buffered HD (001).

Epitaxial relationship

A known issue for the growth of group III-nitrides on the cubic (001) surface of the diamond lattice is the existence of two different wurtzite crystal domains, which are twisted against each other around the *c*-axis by 30° (illustrated as green and red hexagons in Fig. 4a, respectively).[28–30,40,41] Due to the nearly hexagonal shape of the NWs, the statistical distribution of these crystal domains can be estimated. For GaN NWs grown on bare HD (001) (Fig. 4b), 18% of the NWs can be attributed to the first crystal domain (marked in green, $[11\bar{2}0]$GaN‖[110]diamond) and 23% to the second one (marked in red, $[1\bar{1}00]$GaN‖[110] diamond). Nevertheless, as is shown by the XRD measurements below, the almost equal distribution of the crystal domains is deceiving, *i.e.*, the green-marked domain prevails. This might be due to the indistinct shape or tilting of the other NWs, where an attribution was not possible. In contrast, when grown on an AlN buffer the NWs preferentially show a certain orientation: 45% of the NWs can be attributed to the green domain and only 7% to the red one (Fig. 4c). 48% of the NWs tend to have an indistinct shape. Note that the SEM images are aligned with the crystallographic orientation depicted in Fig. 4a with the off-cut direction pointing to the top of the images and the polishing grooves of the diamond surface parallel to [100]diamond.

In order to quantify the large-area crystal domain distribution, XRD measurements were performed. Fig. 5a shows a 360° ϕ-scan of the $(\bar{1}103)$ reflex of GaN NWs grown on bare HD (001). A clear preference for the $[11\bar{2}0]$GaN‖[110]diamond domain (marked in green in accordance with the color code used in

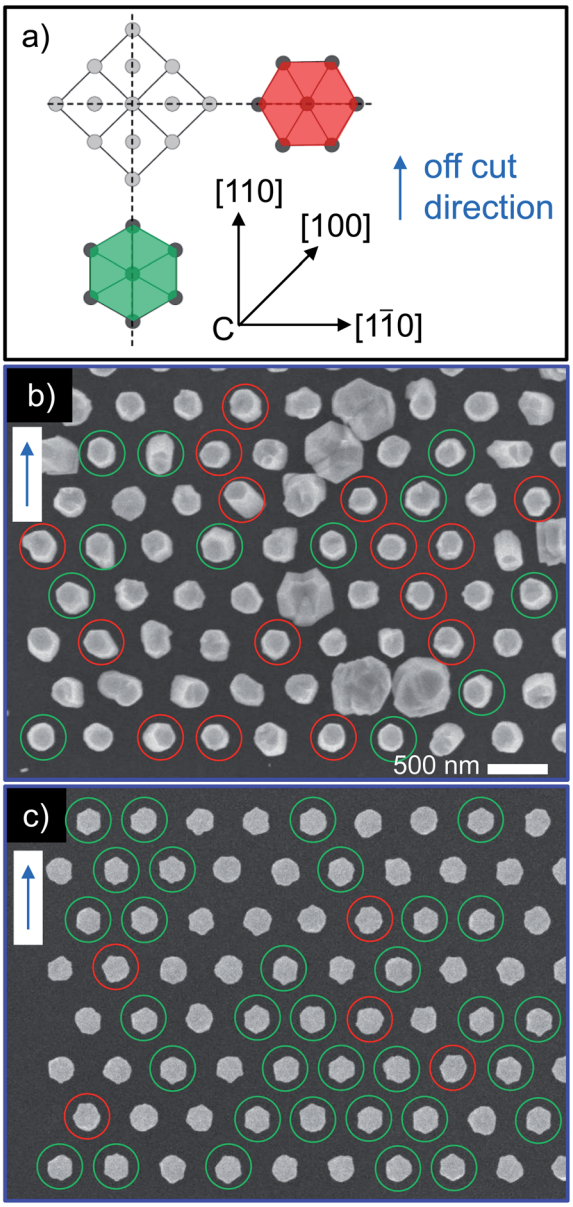

Fig. 4 (a) Schematic drawing of the in-plane epitaxial relationship of the wurtzite lattice on the diamond (001) surface with two possible crystal domains, [11$\bar{2}$0]GaN||[110]diamond (green hexagon) and [1$\bar{1}$00]GaN||[110]diamond (red hexagon). Top view SEM images of GaN NWs on HD (001) (b) without and (c) with the AlN buffer layer. The red and green circles mark the NWs which can be attributed to the corresponding crystal domains in (a). The blue arrows mark the off-cut direction of the HD (001).

Fig. 4a can be found with an average peak height ratio of 2.1 : 1. Similar results were obtained for GaN NWs grown on an AlN buffer with an average peak height ratio of 1.7 : 1. The thin AlN buffer does not significantly influence the domain distribution of the GaN NWs.

As the polishing grooves are along [100]diamond they cannot break the symmetry of the diamond surface, which would lead to a preferential growth of a certain crystal domain. Thus, only the off-cut direction is the decisive factor for the in-plane orientation the GaN NWs. A favoring of the [11$\bar{2}$0]GaN||[11$\bar{2}$0]AlN||[110]diamond domain with a surface off-cut in [110] is in accordance with epitaxial GaN[41] and AlN[30] layers on diamond (001) reported in the literature. Furthermore, it is in agreement with studies investigating the growth of group-III nitrides on Si (001).[42–44] For both substrate materials it was observed that large off-cut angles lead to single domain growth of GaN (AlN). While an off-cut in the ⟨100⟩ direction did not influence the domain formation of wurtzite group-III nitrides, an off-cut parallel to ⟨110⟩ enhanced the formation of one domain. Nominally (001) surfaces with very small off-cut angles consist of single-atomic-step terraces where the orientation of the C–C (Si–Si) dimers at the steps alternate for adjacent terraces, resulting in no favorable wurtzite domain formation. High off-cut angles increase the possibility of double-height-atomic step formation, resulting in a preferred orientation of the C–C (Si–Si) dimers favoring single domain growth.

It has to be noted that for Si (001) substrates off-cut angles > 4° are sufficient to suppress double domain growth[42–44] while on diamond (001) substrates either extremely large (>11°) off-cut angles[41] or a post-deposition annealing at 1700 °C (off-cut angle of approx. 3°)[30] was necessary to stabilize a single crystal domain, respectively. The more complicated epitaxy on diamond (001) might be due to its surface roughness. In the discussed literature no information about the roughness of the substrate surfaces can be found. Deep polishing grooves of the diamond surfaces like in Fig. 1a might disturb the formation of double-height-atomic steps and, thus, counteract single domain formation. Nevertheless, polishing grooves parallel to ⟨110⟩ could enhance the highly oriented AlN (GaN) growth acting as an "artificially patterned" substrate like in pseudoepitaxy.[41,45] A study investigating the interplay of polishing direction, surface smoothness and off-cut angle/direction is needed to fully understand the nucleation mechanisms. Furthermore, pre-treatments like high temperature annealing might stabilize a certain wurtzite domain on diamond (001) like already shown for the growth on Si (001).[42]

In order to investigate the epitaxial relationship of GaN NWs on HD (001) in more detail, reciprocal space maps (RSMs) were recorded. The RSM of GaN NWs with an AlN buffer is shown in Fig. 5c. The symmetric (0002) and (0004) reflexes of GaN can be clearly seen and the asymmetric ($\bar{1}$101), (1$\bar{1}$02) and (1$\bar{1}$03) reflexes are identifiable as expected. In addition, the (2$\bar{1}$12) reflex is visible. This verifies the double domain growth of GaN on HD (001) as this peak would be otherwise forbidden for $\phi = 0°$. The symmetric (004) reflex of diamond can be seen as well as its asymmetric (1$\bar{1}$3) and (1$\bar{1}$1) reflexes. Moreover, the forbidden (222) reflex of diamond was detectable with a significantly lower intensity compared to all other diamond peaks. The large broadening of the peaks in angular direction is caused by the non-monochromatic X-ray source used. In particular, the satellite peaks at lower 2θ angles of the (004) and the ($\bar{1}$13) reflexes are a consequence of the CuK_β-radiation of the X-ray tube. Most importantly, the diamond lattice is rotated by 5° around the χ-axis with respect to the GaN lattice. This can be explained by the off-cut of the HD (001) substrates. The NWs do not align with the diamond lattice but grow perpendicular to

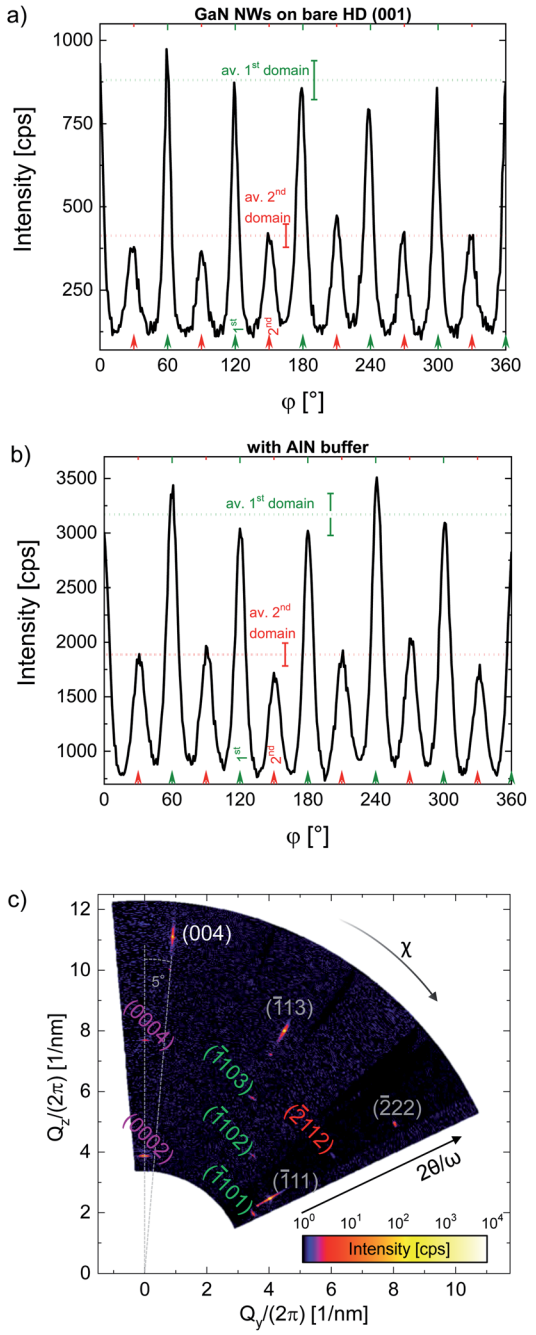

Fig. 5 XRD of GaN NWs on HD (001): ϕ-scan of the asymmetric (1̄103) reflex of GaN NWs on (a) bare diamond and (b) with the AlN buffer layer. (c) RSM of GaN NWs grown on AlN-buffered HD (001). The symmetric GaN (diamond) reflexes are labeled in violet (white), while the asymmetric ones are labeled in green and red (gray). The dashed gray lines indicate the angle between [0001]GaN and [001]diamond.

the polished surface. This also applies to GaN NWs on bare HD (001) (not shown). This tilt between the substrate and the epitaxial group-III nitride layers due to the off-cut was also reported for the growth on Si and diamond (001) in the literature. The tilting may reduce the interface energy of the heterostructure due to a reduction of the lattice mismatch.[28,42–44] This behavior is in contrast to the growth on SCD (111) where the group-III nitride layers and NWs are aligned along the diamond lattice.[28,35] Additionally, this can be seen in Fig. 2a, where all GaN NWs are tilted with respect to the SCD (111) surface in the same direction.

Polarity of GaN NSs on diamond

GaN NWs nucleate with mixed polarity on SCD (111), where both polarity types can be controlled up to a fraction of 93% by pre-treatments like plasma exposure and the variation of the substrate temperature during MBE.[33] In addition, by deposition of a 10 nm thick AlN layer prior to the SAG of GaN NWs, a yield of 100% Ga-polar NWs has been demonstrated.[46] Here, the polarity of GaN NSs on HD (001) with and without AlN buffer is evaluated by polarity-selective wet chemical etching and KPFM.

Fig. 6a and b show the height and corresponding surface potential map of a GaN NW array on AlN-buffered HD (001). The individual NWs can be resolved and they have an equal height and diameter. All top facets of the NWs have about the same surface potential, confirming their area-wide uni-polar growth in contrast to GaN NWs on bare SCD (111) where potential differences of up to 700 mV have been observed for NWs of different polarities.[33] Nevertheless, from this top scan it cannot be extracted which polarity the NWs have as the absolute surface potential values vary significantly in the literature, even in their sign.[47,48] Thus, a KPFM measurement of a single NW lying on the substrate was performed. The growth direction of the NW can be taken from the height scan (Fig. 6c, indicated by the white arrow) where the pyramidal top facet is identified on the right side of the image. The angle of the semi-polar facet relative to the *c*-plane can be determined to be approx. 35°. The corresponding KPFM map (Fig. 6d) shows a relatively low surface potential at the NW bottom, which increases towards the NW top. This becomes more evident in the plot of a section along the NW, the direction of which is marked by the arrow in Fig. 6d. The blue graph in Fig. 6e depicts the height information and yields the NW dimensions (marked in gray). The surface potential depicted in red drops from approx. 350 mV on the substrate to −120 mV at the NW bottom. At the NW top the potential increases to over 500 mV. A higher surface potential at the NW top corresponds to a Ga-polar NW in this study as discussed for the same setup and measurement technique in earlier work.[33]

An aqueous potassium hydroxide (KOH) solution selectively etches the N-polar facets of GaN NWs, while the Ga-polar planes remain unaffected.[33,49,50] This provides the possibility to investigate the polarity of GaN NSs by selective etching as a complementary, less time consuming method than KPFM, which probes a large area of GaN NSs. Images of the GaN NSs before and after the KOH treatment for comparison are shown in the ESI.†

Fig. 7a shows GaN NWs on AlN-buffered HD (001) after the etching process. The height of the NSs decreased by approx. 40 nm and the average NS width by almost 100 nm. The etched NWs have a stepped cone-like shape with increasing NW diameter from the top to the bottom. This is ascribed to etching

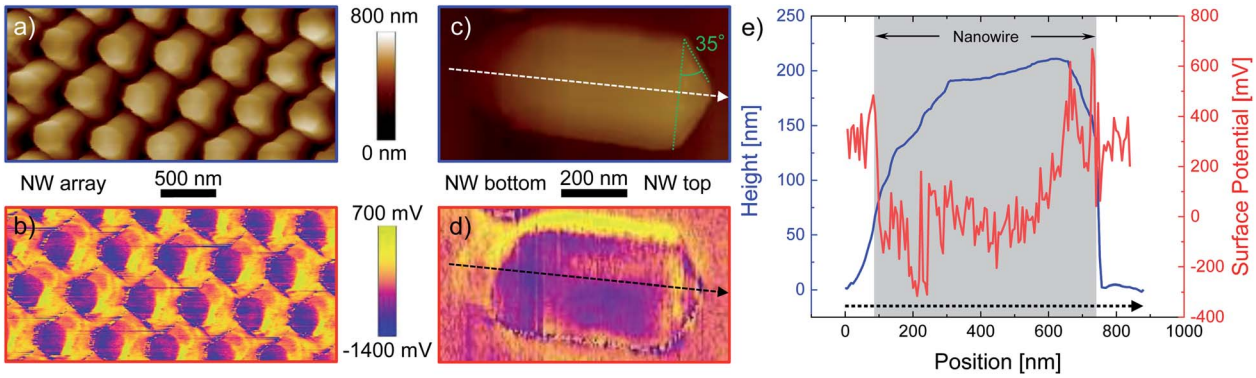

Fig. 6 KPFM of GaN NWs grown on AlN-buffered HD (001): (a and b) topology and surface potential map of an array of free-standing NWs and (c and d) those of a single lying NW. The dashed lines mark the position of the line scans of the height profile and potential depicted in (e). The dashed arrows point from the bottom to the top of the NW.

of the semi-polar NW top facets down to stable Ga-polar *c*-planes, and non-polar *a*-/*m*-planes form as illustrated in Fig. 7b. A comparable etching mechanism has been reported for pencil-like Ga-polar NWs.[50] In the case of GaN NFs, the etching leads to a *c*-plane top facet (*cf.* Fig. S5, ESI†). The etching mechanism becomes most obvious in Fig. 7c. Here, a single lying NW is shown, which lies flat on the substrate before the KOH treatment. Consequently, the top and bottom of the NW were exposed to the etchant. While at the NW bottom pyramidal structures evolve, which is a clear sign of N-polarity of this facet,[50–52] the NW top shows a staircase-like structure.

Fig. 7d and e show GaN NWs on HD (001) without the AlN buffer layer after KOH etching. The etched NWs are thinner but not significantly shorter. A lateral etch rate of approx. 40 nm min^{-1} was determined. Moreover, all NWs show signs of etching at the bottom. This can be explained by a lateral growth over the Ti mask with no direct contact to it. Thus, the facets at the NW bottom are exposed to the KOH solution as observed for GaN NWs on bare SCD (111).[33] The same effect can be observed for etched GaN NFs on bare HD (001) (Fig. 7f), which creates the impression of NFs hovering over their Ti mask openings.

Thus, we conclude that independently of the presence of an AlN buffer layer, GaN NSs on HD (001) nucleate exclusively Ga-polar in contrast to their counterparts on SCD (111), where pure Ga-polar growth is only achieved with an AlN buffer. The unipolar growth of GaN NSs on HD (001) is an important advantage over the growth on SCD (111) when it comes to applications in, *e.g.*, optoelectronics and high-power electronics.

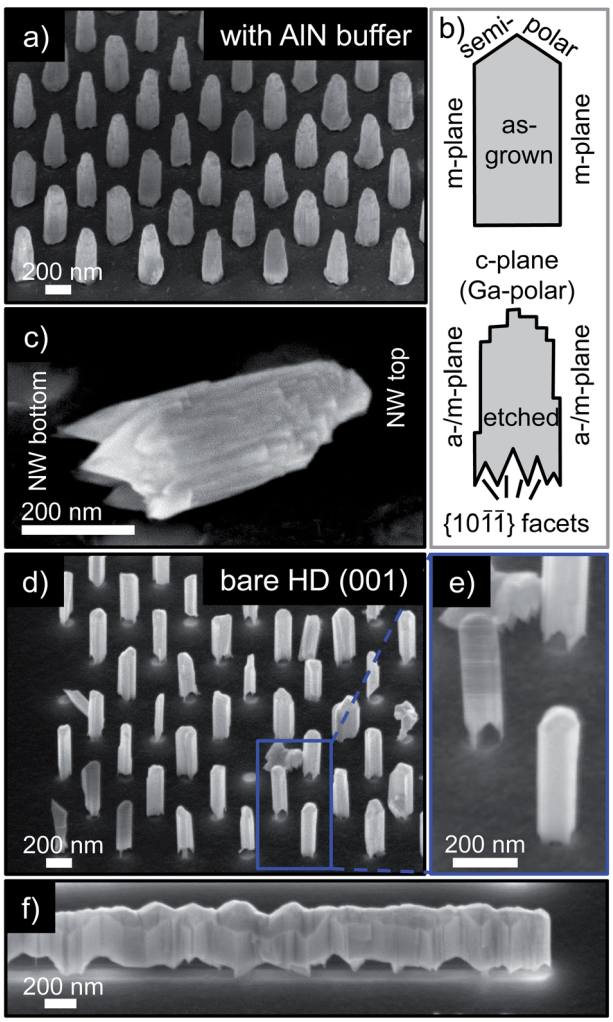

Fig. 7 45°-tilted view SEM images of KOH etched GaN NSs: (a) NW array on AlN-buffered HD (001). (b) Schematic sketch of the etching morphology. (c) Single, lying NW grown on AlN-buffered HD (001), which exposed the NW top and bottom to the hot KOH. (d) NW array on bare HD (001). (e) A magnified image of the three NWs shown in (d). (f) A NF on bare HD (001) after KOH etching.

Photoluminescence properties

The structural quality of the GaN NSs grown on the different diamond substrates was analyzed by low temperature PL measurements shown in Fig. 8. The dominant emission of all NWs (Fig. 8a) is at 3.47 eV, which corresponds to the donor-bound exciton recombination (D^0X) *via* the A valence band in GaN.[35,53,54] The low-energy shoulder of this main emission at approx. 3.45 eV is most likely attributed to polarity inversion domain boundaries (IDBs),[24,54,55] which are present in all investigated NWs. The luminescence in the 3.40–3.43 eV region is attributed to basal plane stacking faults

(BSFs).[24,36,55–57] While almost no indications of BSFs are visible for GaN NWs on SCD (111) and AlN-buffered HD (001), a distinct peak, which is centered around 3.41 eV can be seen for GaN NWs on bare HD (001). The NWs on SCD (111) show an additional luminescence at 3.35 eV in accordance to previously reported results.[32] This emission can possibly be attributed to *m*-plane stacking faults (MSFs) and is a consequence of a distinct lateral growth of the NSs.[32,37,54] An emission from donor–acceptor pairs (DAPs) is visible in the region around 3.27 eV with weak LO phonon replica at lower energies shifted by 92 meV. The exact DAP emission energy depends on the ionization energies of the involved donors and acceptors. Oxygen seems to be a likely donor in the GaN NWs. Carbon impurities arising from the substrate as well as point defects like Ga-vacancies might act as acceptors.[54] The GaN NWs on the AlN buffer exhibit the lowest defect emission of all investigated samples.

Fig. 8b shows the PL spectra of the GaN NFs. On HD (001), the NFs show their most pronounced emission at 3.47 eV (D^0X). In contrast, for NFs on SCD (111) mainly an emission related to IDBs is observed. This might be explained by the nucleation of GaN NSs on SCD (111). On this diamond surface, NSs can nucleate with both polarities.[33] As these seeds nucleate to approx. 45% N-polar,[33] a lot of IDBs emerge during the NF coalescence. In contrast, when grown on HD (001), the NSs nucleate exclusively Ga-polar. Consequently, fewer IDBs are present in NFs on this substrate. A possible origin of these residual IDBs is contaminations arising from the Ti mask fabrication process triggering N-polar nucleation. Blanchard *et al.* showed that even in homo-epitaxy of GaN NWs monolayer contaminations can lead to the formation of IDBs.[58] However, the number of IDBs must be very limited as no signs of them were observed by polarity-selective etching. Future transmission electron microscopy studies combined with energy-dispersive X-ray spectroscopy of the GaN/HD and GaN/AlN/HD interfaces might shed more light on this issue. Nevertheless, due to the rough surface of the HD investigated in this article an extensive TEM study might be premature. Similar to the GaN NW spectra, only NFs on bare HD (001) show a pronounced emission attributable to BSFs. It has to be noted that the position of the peak is shifted to 3.42 eV instead of 3.41 eV in the case of NWs. The exact emission energy from BSFs, which are ideal crystal phase quantum wells,[57,59] is influenced by polarization fields and strain, and, additionally, by the size of the stacking faults.[36] As the D^0X emissions of GaN NWs and NFs on bare HD (001) are exactly at the same position, strain can be excluded. Thus, the 0.01 eV blue shift of the NFs can be explained by a larger extension of the stacking faults due to the 2D architecture of the fins compared to the more laterally confined NWs. In contrast to the NW spectra, MSFs are only visible for NFs on AlN-buffered HD (001). The appearance of MSFs might be caused by imperfections of the Ti mask influencing the extent of the lateral growth rather than the actual substrate. Finally, the NFs on SCD (111) and AlN-buffered HD (001) show a DAP emission similar to their NW counterparts.

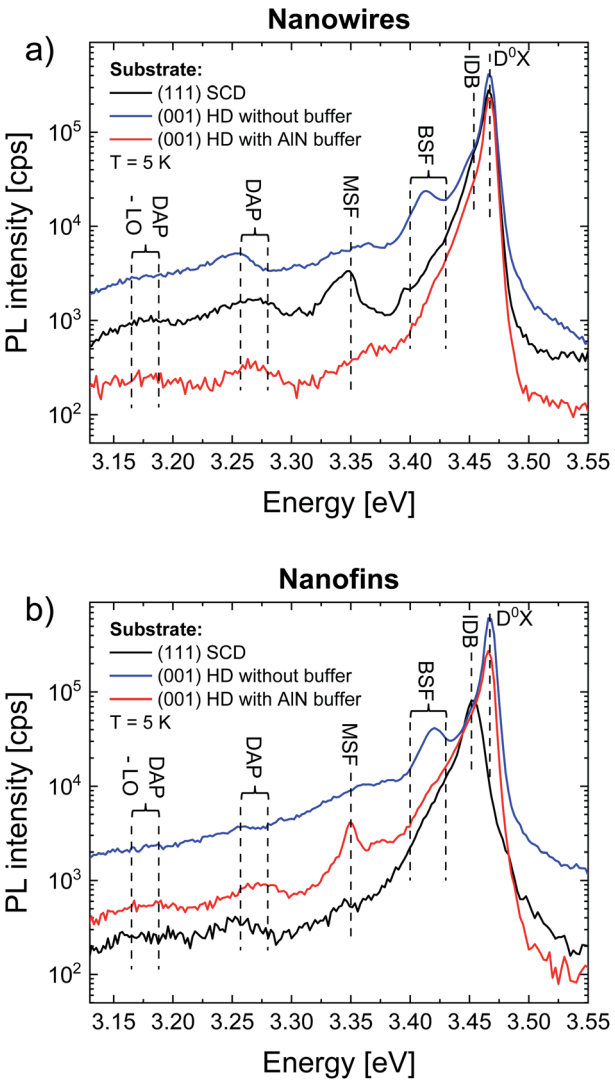

Fig. 8 Low temperature PL spectra of the near-band edge region of GaN (a) NWs and (b) NFs grown on bare SCD (111) (black), bare HD (001) (blue) and AlN-buffered HD (001) (red). The dashed lines mark the emissions attributed to the donor-bound exciton recombination (D^0X), polarity inversion domain boundaries (IDBs), basal plane stacking faults (BSFs), *m*-plane stacking faults (MSFs), and donor–acceptor pairs (DAPs) with their characteristic LO phonon replica.

Experimental section

Group III-nitrides were grown on diamond substrates with a size of 3 × 3 mm^2. Commercial SCD (type chemical vapor deposition (CVD) IIa) with (111) surface orientation and a thickness of 0.5 mm was purchased from Element Six Ltd. HD (001) was purchased from Augsburg Diamond Technology GmbH. These diamonds were grown by means of CVD on Si (001)/yttria-stabilized zirconia (001)/Ir substrates (001).[60] After substrate removal, free-standing 1 mm thick HD (001) was obtained. The SCD are characterized characterized by very high crystal quality with a 2θ full width at half maximum (FWHM) of the (111) reflex of 0.006° and a ω-rocking curve FWHM of 0.003°. The HDs have a 2θ FWHM of the (004) reflex of 0.106° and a ω-

rocking curve FWHM of 0.058°. The corresponding XRD data and AFM images of the diamond surfaces are provided in the ESI.† All diamond substrates have an intentional off-cut of approx. 5°.

The back of all diamonds was coated with 200 nm Ti followed by 70 nm Pt in order to enhance the heat absorption from the radiative heater during MBE growth. Note that the given substrate temperatures in this work refer to thermocouple values of the substrate heater, which overestimate the real temperatures at the diamond surface.

Planar AlN buffer layers were grown *via* MBE on HD (001). To this end, the diamond substrates were exposed to an oxygen plasma at 200 W for 5 min prior to mounting them into the MBE system in order to guarantee a reproducible and uniform surface termination. This step is followed by a nitridation of the diamond surface in the MBE chamber *via* exposure to a nitrogen plasma with a N_2 flux of 0.600 sccm and a radio frequency (RF) power of 300 W for 15 min at 400 °C. The AlN growth was conducted at a substrate temperature of 770 °C and an Al flux of 2.8×10^{-7} mbar beam equivalent pressure (BEP) at constant nitrogen supply. After MBE, the samples were etched in hydrochloric acid (36%) for 5 min and cleaned in an acetone ultrasonic bath for 5 min and with isopropyl alcohol in order to remove potential Al clusters on the surface.

The GaN NSs investigated in this work were grown *via* MBE in a SAG mode. To this end, 7–10 nm of Ti were evaporated onto the sample surface as a mask material. In order to enhance the sticking of the Ti, the bare diamonds were exposed to an oxygen plasma (200 W, 5 min) beforehand. By means of electron beam lithography, the Ti mask was patterned with arrays of holes and lines, which serve as nucleation spots for the NW and NF growth, respectively. Prior to the MBE growth, the bare diamond substrates were again exposed to oxygen plasma in order to get a well-defined surface. When growing the NSs on an AlN buffer, this plasma treatment was replaced by an etching of the sample with hydrochloric acid to remove the native surface oxide. The MBE growth was initiated with a nitridation of the samples by exposure to a nitrogen plasma with a flux of 0.363 sccm and a power of 425 W at 400 °C and 800 °C for 10 and 5 min, respectively. This leads to the conversion of the Ti mask into a more stable TiN layer. The actual GaN NS growth under equal plasma conditions and a Ga flux of 1.0×10^{-6} mbar BEP was performed at a substrate temperature of 880 °C (900 °C, 940 °C) for the bare HD (AlN-buffered HD, SCD). A detailed description of the NS fabrication process can be found in previous publications.[31,32,34] The background pressure of the MBE system was in the 10^{-10} mbar range.

(High resolution) XRD measurements were performed with a Rigaku SmartLab X-ray diffractometer using a Cu cathode operating at 40 kV. A Ge double-bounce monochromator to select the $CuK_{\alpha 1}$ emission line ($\lambda = 1.54059$ Å) and a HyPix3000 CCD detector in point (0D) mode were used for the high resolution XRD measurements of the diamond substrates. ϕ-scans of the GaN NSs on diamond and X-ray reflectivity measurements of the AlN buffer layer were carried out without a monochromator. RSMs of the samples were recorded without a monochromator in 1D detector mode, which enables the measurement of the diffraction intensities with an angular range of 2θ (χ-step).

For the PL measurements a quadrupled Nd:YAG laser with a wavelength of 266 nm in continuous wave operation was used for the above-band gap excitation of the GaN NSs. The light was guided by a convergent lens with a focal length of 70 mm into an Oxford Instruments He flow cryostat, resulting in a spot size of approx. 50 μm on the sample surface. The excitation power was set to 50 W cm^{-2}. The PL signal was spectrally filtered using a DILOR double spectrometer with a focal length of 800 mm and detected using a Peltier-cooled photo-multiplier tube with a dark count rate of 15 counts per second (cps).

Polarity-selective wet chemical etching was performed with 0.5 M KOH in deionized water at 85 °C. The surface contact potential difference of the GaN NSs was measured with a Bruker MultiMode 8 AFM using a PeakForce frequency-modulated KPFM technique in a dual pass mode. The AFM probes (Bruker "PFQNE-AL") used had a Si tip with a triangular shape. All KPFM measurements were performed in the dark under ambient conditions. A detailed description of the setup is described in an earlier publication.[33]

Summary and conclusion

In summary, GaN nanostructures (NSs) on heteroepitaxially grown diamond (HD) (001) substrates were grown *via* selective area growth (SAG) by plasma-assisted molecular beam epitaxy (MBE) with and without an AlN buffer layer. When grown on bare HD (001), the NSs show a comparable appearance as on single crystalline diamond (SCD) (111). On AlN-buffered HD (001), the NSs have the most uniform morphology with good control over the NS dimensions. The GaN nanowires (NWs) nucleate in two different crystal domains on HD (001), which are in-plane rotated against each other by 30°. We observe a favoring of the [11$\bar{2}$0]GaN||[11$\bar{2}$0]AlN||[110]diamond domain, which is caused by the substrate off-cut in the [110] direction. In contrast to the growth on SCD, the NWs grow perpendicular to the off-cut diamond surface, *i.e.*, the *c*-axis of GaN is tilted by approx. 5° with respect to [001]diamond. By polarity-selective wet chemical etching and Kelvin probe force microscopy (KPFM) measurements we showed that GaN NSs nucleate solely Ga-polar on HD (001) with and without AlN buffer. Low temperature photoluminescence (PL) measurements indicate good quality of the NSs grown on different diamond substrates, with GaN NSs on AlN-buffered HD (001) being most promising in terms of a low defect luminescence.

Conflicts of interest

There are no conflicts to declare.

Acknowledgements

This work was funded by the Deutsche Forschungsgemeinschaft (DFG, German Research Foundation) under Germany's Excellence Strategy – EXC 2089/1 – 390776260 (e-conversion) and the Bavarian program Solar Energies Go

Hybrid (SolTech). It was supported by the Deutsche Forschungsgemeinschaft (DFG) through the TUM International Graduate School of Science and Engineering (IGSSE), GSC 81. We thank C.-M. Jiang for his valuable help with the XRD measurements.

References

1 J. Kamimura, P. Bogdanoff, J. Laehnemann, C. Hauswald, L. Geelhaar, S. Fiechter and H. Riechert, Photoelectrochemical Properties of In, (In,Ga)N Nanowires for Water Splitting Investigated by *in situ* Electrochemical Mass Spectroscopy, *J. Am. Chem. Soc.*, 2013, **135**, 10242–10245.

2 P. Varadhan, H.-C. Fu, D. Priante, J. R. D. Retamal, C. Zhao, M. Ebaid, T. K. Ng, I. Ajia, S. Mitra, I. S. Roqan, *et al.*, Surface Passivation of GaN Nanowires for Enhanced Photoelectrochemical Water-Splitting, *Nano Lett.*, 2017, **17**, 1520–1528.

3 L. Zhang, Y. Li, X. Xiu, G. Xin, Z. Xie, T. Tao, B. Liu, P. Chen, R. Zhang and Y. Zheng, Preparation of Vertically Aligned GaN@Ga_2O_3 Core–Shell Heterostructured Nanowire Arrays and Their Photocatalytic Activity for Degradation of Rhodamine B, *Superlattices Microstruct.*, 2020, **143**, 106556.

4 R. Calarco, T. Stoica, O. Brandt and L. Geelhaar, Surface-Induced Effects in GaN Nanowires, *J. Mater. Res.*, 2011, **26**, 2157.

5 J. Teubert, P. Becker, F. Furtmayr and M. Eickhoff, GaN Nanodiscs Embedded in Nanowires as Optochemical Transducers, *Nanotechnology*, 2011, **22**, 275505.

6 K. Maier, A. Helwig, G. Müller, J. Schörmann and M. Eickhoff, Photoluminescence Detection of Surface Oxidation Processes on InGaN/GaN Nanowire Arrays, *ACS Sens.*, 2018, **3**, 2254–2260.

7 M. Hetzl, M. Kraut, T. Hoffmann, J. Winnerl, K. Boos, A. Zeidler, I. D. Sharp and M. Stutzmann, A Systematic Investigation of Radiative Recombination in GaN Nanowires: The Influence of Nanowire Geometry and Environmental Conditions, *J. Appl. Phys.*, 2018, **124**, 035704.

8 R. Koester, D. Sager, W.-A. Quitsch, O. Pfingsten, A. Poloczek, S. Blumenthal, G. Keller, W. Prost, G. Bacher and F.-J. Tegude, High-Speed GaN/GaInN Nanowire Array Light-Emitting Diode on Silicon (111), *Nano Lett.*, 2015, **15**, 2318–2323.

9 B. O. Jung, S.-Y. Bae, S. Lee, S. Y. Kim, J. Y. Lee, Y. Honda and H. Amano, Emission Characteristics of InGaN/GaN Core–Shell Nanorods Embedded in a 3D Light-Emitting Diode, *Nanoscale Res. Lett.*, 2016, **11**, 1–10.

10 M. Philip, D. Choudhary, M. Djavid, K. Le, J. Piao and H. Nguyen, High Efficiency Green/Yellow and Red InGaN/AlGaN Nanowire Light-Emitting Diodes Grown by Molecular Beam Epitaxy, *J. Sci.: Adv. Mater. Devices*, 2017, **2**, 150–155.

11 X. Dai, A. Messanvi, H. Zhang, C. Durand, J. Eymery, C. Bougerol, F. H. Julien and M. Tchernycheva, Flexible Light-Emitting Diodes Based on Vertical Nitride Nanowires, *Nano Lett.*, 2015, **15**, 6958–6964.

12 N. Sone, A. Suzuki, H. Murakami, N. Goto, M. Terazawa, W. Lu, D.-P. Han, K. Iida, M. Ohya, M. Iwaya, *et al.*, Improved Uniform Current Injection into Core–Shell-Type GaInN Nanowire Light-Emitting Diodes by Optimizing Growth Condition and Indium-Tin-Oxide Deposition, *Phys. Status Solidi A*, 2020, **217**, 1900715.

13 M. Nami, A. Rashidi, M. Monavarian, S. Mishkat-Ul-Masabih, A. K. Rishinaramangalam, S. R. Brueck and D. Feezell, Electrically Injected GHz-Class GaN/InGaN Core–Shell Nanowire-Based μLEDs: Carrier Dynamics and Nanoscale Homogeneity, *ACS Photonics*, 2019, **6**, 1618–1625.

14 H. Q. T. Bui, R. T. Velpula, B. Jain, O. H. Aref, H.-D. Nguyen, T. R. Lenka and H. P. T. Nguyen, Full-Color InGaN/AlGaN Nanowire Micro Light-Emitting Diodes Grown by Molecular Beam Epitaxy: A Promising Candidate for Next Generation Micro Displays, *Micromachines*, 2019, **10**, 492.

15 M. F. Fatahilah, K. Strempel, F. Yu, S. Vodapally, A. Waag and H. S. Wasisto, 3D GaN Nanoarchitecture for Field-Effect Transistors, *Microsyst. Nanoeng.*, 2019, **3**, 59–81.

16 K. Strempel, F. Römer, F. Yu, M. Meneghini, A. Bakin, H.-H. Wehmann, B. Witzigmann and A. Waag, Vertical 3D Gallium Nitride Field-Effect Transistors Based on Fin Structures with Inverted p-Doped Channel, *Semicond. Sci. Technol.*, 2020, **36**, 014002.

17 C.-T. Lee and J.-C. Guo, Fin-Gated Nanochannel Array Gate-Recessed AlGaN/GaN Metal-Oxide-Semiconductor High-Electron-Mobility Transistors, *IEEE Trans. Electron Devices*, 2020, **67**, 1939–1945.

18 K.-S. Im, S. J. An, C. G. Theodorou, G. Ghibaudo, S. Cristoloveanu and J.-H. Lee, Effect of Gate Structure on the Trapping Behavior of GaN Junctionless FinFETs, *IEEE Electron Device Lett.*, 2020, **41**, 832–835.

19 M. Wu, X.-H. Ma, L. Yang, M. Zhang, Q. Zhu, X.-C. Zhang, B. Hou, X.-F. Zheng and Y. Hao, Investigation of the Nanochannel Geometry Modulation on Self-Heating in AlGaN/GaN Fin-HEMTs on Si, *Appl. Phys. Lett.*, 2019, **115**, 083505.

20 G. Doundoulakis, A. Adikimenakis, A. Stavrinidis, K. Tsagaraki, M. Androulidaki, F. Iacovella, G. Deligeorgis, G. Konstantinidis and A. Georgakilas, Nanofabrication of Normally-Off GaN Vertical Nanowire MESFETs, *Nanotechnology*, 2019, **30**, 285304.

21 V. Consonni, M. Knelangen, L. Geelhaar, A. Trampert and H. Riechert, Nucleation Mechanisms of Epitaxial GaN Nanowires: Origin of Their Self-Induced Formation and Initial Radius, *Phys. Rev. B: Condens. Matter Mater. Phys.*, 2010, **81**, 085310.

22 M. Hugues, P. Shields, F. Sacconi, M. Mexis, M. Auf der Maur, M. Cooke, M. Dineen, A. Di Carlo, D. Allsopp and J. Zúñiga-Pérez, Strain Evolution in GaN Nanowires: From Free-Surface Objects to Coalesced Templates, *J. Appl. Phys.*, 2013, **114**, 084307.

23 K. Kishino and S. Ishizawa, Selective-Area Growth of GaN Nanocolumns on Si (111) Substrates for Application to Nanocolumn Emitters with Systematic Analysis of Dislocation Filtering Effect of Nanocolumns, *Nanotechnology*, 2015, **26**, 225602.

24 P. Aseev, Ž. Gačević, A. Torres-Pardo, J. González-Calbet and E. Calleja, Improving Optical Performance of GaN Nanowires Grown by Selective Area Growth Homoepitaxy: Influence of Substrate and Nanowire Dimensions, *Appl. Phys. Lett.*, 2016, **108**, 253109.

25 M. J. Tadjer, T. J. Anderson, J. C. Gallagher, P. E. Raad, P. Komarov , A. D. Koehler, K. D. Hobart and F. J. Kub, Thermal Performance Improvement of GaN-on-Diamond High Electron Mobility Transistors, in *2018 76th Device Research Conference (DRC)*, Santa Barbara, 2018, pp. 1–2.

26 Z. Cheng, F. Mu, L. Yates, T. Suga and S. Graham, Interfacial Thermal Conductance across Room-Temperature-Bonded GaN/Diamond Interfaces for GaN-on-Diamond Devices, *ACS Appl. Mater. Interfaces*, 2020, **12**, 8376–8384.

27 A. El Helou, P. Komarov, M. J. Tadjer, T. J. Anderson, D. A. Francis, T. Feygelson, B. B. Pate, K. D. Hobart and P. E. Raad, High-Resolution Thermoreflectance Imaging Investigation of Self-Heating in AlGaN/GaN HEMTs on Si, SiC, and Diamond Substrates, *IEEE Trans. Electron Devices*, 2020, **67**, 5415–5420.

28 G. Vogg, C. Miskys, J. Garrido, M. Hermann, M. Eickhoff and M. Stutzmann, High Quality Heteroepitaxial AlN Films on Diamond, *J. Appl. Phys.*, 2004, **96**, 895–902.

29 M. Imura, K. Nakajima, M. Liao, Y. Koide and H. Amano, Growth Mechanism of *c*-Axis-Oriented AlN on (0 0 1) Diamond Substrates by Metal–Organic Vapor Phase Epitaxy, *J. Cryst. Growth*, 2010, **312**, 368–372.

30 T. Shirato, Y. Hayashi, K. Uesugi, K. Shojiki and H. Miyake, High-Temperature Annealing of Sputter-Deposited AlN on (001) Diamond Substrate, *Phys. Status Solidi B*, 2020, **257**, 1900447.

31 F. Schuster, M. Hetzl, S. Weiszer, J. A. Garrido, M. De La Mata, C. Magen, J. Arbiol and M. Stutzmann, Position-Controlled Growth of GaN Nanowires and Nanotubes on Diamond by Molecular Beam Epitaxy, *Nano Lett.*, 2015, **15**, 1773–1779.

32 M. Hetzl, F. Schuster, A. Winnerl, S. Weiszer and M. Stutzmann, Reprint of: GaN Nanowires on Diamond, *Mater. Sci. Semicond. Process.*, 2016, **55**, 32–45.

33 M. Hetzl, M. Kraut, T. Hoffmann and M. Stutzmann, Polarity Control of Heteroepitaxial GaN Nanowires on Diamond, *Nano Lett.*, 2017, **17**, 3582–3590.

34 J. Winnerl, M. Kraut, S. Artmeier and M. Stutzmann, Selectively Grown GaN Nanowalls and Nanogrids for Photocatalysis: Growth and Optical Properties, *Nanoscale*, 2019, **11**, 4578–4584.

35 F. Schuster, F. Furtmayr, R. Zamani, C. Magén, J. R. Morante, J. Arbiol, J. A. Garrido and M. Stutzmann, Self-Assembled GaN Nanowires on Diamond, *Nano Lett.*, 2012, **12**, 2199–2204.

36 A. Urban, M. Müller, C. Karbaum, G. Schmidt, P. Veit, J. Malindretos, F. Bertram, J. Christen and A. Rizzi, Optical Emission of Individual GaN Nanocolumns Analyzed with High Spatial Resolution, *Nano Lett.*, 2015, **15**, 5105–5109.

37 M. Kraut, F. Pantle, J. Winnerl, M. Hetzl, F. Eckmann, I. D. Sharp and M. Stutzmann, Photo-Induced Selective Etching of GaN Nanowires in Water, *Nanoscale*, 2019, **11**, 7967–7975.

38 Z. Gacevic, D. Gomez Sanchez and E. Calleja, Formation Mechanisms of GaN Nanowires Grown by Selective Area Growth Homoepitaxy, *Nano Lett.*, 2015, **15**, 1117–1121.

39 H. Li, L. Geelhaar, H. Riechert and C. Draxl, Computing Equilibrium Shapes of Wurtzite Crystals: The Example of GaN, *Phys. Rev. Lett.*, 2015, **115**, 085503.

40 C. Miskys, J. Garrido, M. Hermann, M. Eickhoff, C. Nebel, M. Stutzmann and G. Vogg, Structural and Interface Properties of an AlN Diamond Ultraviolet Light Emitting Diode, *Appl. Phys. Lett.*, 2004, **85**, 3699–3701.

41 G. Van Dreumel, P. Tinnemans, A. Van Den Heuvel, T. Bohnen, J. G. Buijnsters, J. Ter Meulen, W. Van Enckevort, P. Hageman and E. Vlieg, Realising Epitaxial Growth of GaN on (001) Diamond, *J. Appl. Phys.*, 2011, **110**, 013503.

42 V. Lebedev, J. Jinschek, J. Kräußlich, U. Kaiser, B. Schröter and W. Richter, Hexagonal AlN Films Grown on Nominal and Off-Axis Si (0 0 1) Substrates, *J. Cryst. Growth*, 2001, **230**, 426–431.

43 S. Joblot, E. Feltin, E. Beraudo, P. Vennéguès, M. Leroux, F. Omnès, M. Laügt and Y. Cordier, Hexagonal *c*-Axis GaN Layers Grown by Metalorganic Vapor-Phase Epitaxy on Si (0 0 1), *J. Cryst. Growth*, 2005, **280**, 44–53.

44 F. Schulze, A. Dadgar, J. Bläsing, T. Hempel, A. Diez, J. Christen and A. Krost, Growth of Single-Domain GaN Layers on Si (0 0 1) by Metalorganic Vapor-Phase Epitaxy, *J. Cryst. Growth*, 2006, **289**, 485–488.

45 E. Givargizov, M. Kliya, V. Melik-Adamyan, A. Grebenko, R. DeMattei and R. Feigelson, Artificial Epitaxy (Graphoepitaxy) of Proteins, *J. Cryst. Growth*, 1991, **112**, 758–772.

46 M. Hetzl, J. Wierzbowski, T. Hoffmann, M. Kraut, V. Zuerbig, C. E. Nebel, K. Müller, J. J. Finley and M. Stutzmann, GaN Nanowire Arrays for Efficient Optical Read-Out and Optoelectronic Control of NV Centers in Diamond, *Nano Lett.*, 2018, **18**, 3651–3660.

47 J. Zuniga-Perez, V. Consonni, L. Lymperakis, X. Kong, A. Trampert, S. Fernandez-Garrido, O. Brandt, H. Renevier, S. Keller, K. Hestroffer, *et al.*, Polarity in GaN and ZnO: Theory, Measurement, Growth, and Devices, *Appl. Phys. Rev.*, 2016, **3**, 041303.

48 A. Minj, A. Cros, N. Garro, J. Colchero, T. Auzelle and B. Daudin, Assessment of Polarity in GaN Self-Assembled Nanowires by Electrical Force Microscopy, *Nano Lett.*, 2015, **15**, 6770–6776.

49 X. Wang, S. Li, S. Fündling, J. Wei, M. Erenburg, H.-H. Wehmann, A. Waag, W. Bergbauer, M. Strassburg, U. Jahn, *et al.*, Polarity Control in 3D GaN Structures Grown by Selective Area MOVPE, *Cryst. Growth Des.*, 2012, **12**, 2552–2556.

50 C. Blumberg, P. Häuser, F. Wefers, D. Jansen, F.-J. Tegude, N. Weimann and W. Prost, A Systematic Study of Ga- and N-polar GaN Nanowire–Shell Growth by Metal Organic Vapor Phase Epitaxy, *CrystEngComm*, 2020, **22**, 5522–5532.

51 H. M. Ng, N. G. Weimann and A. Chowdhury, GaN Nanotip Pyramids Formed by Anisotropic Etching, *J. Appl. Phys.*, 2003, **94**, 650–653.
52 J. Weyher, S. Müller, I. Grzegory and S. Porowski, Chemical Polishing of Bulk and Epitaxial GaN, *J. Cryst. Growth*, 1997, **182**, 17–22.
53 G. Chen, M. Smith, J. Lin, H. Jiang, S.-H. Wei, M. Asif Khan and C. Sun, Fundamental Optical Transitions in GaN, *Appl. Phys. Lett.*, 1996, **68**, 2784–2786.
54 M. A. Reshchikov and H. Morkoç, Luminescence Properties of Defects in GaN, *J. Appl. Phys.*, 2005, **97**, 5–19.
55 T. Auzelle, B. Haas, M. Den Hertog, J.-L. Rouvière, B. Daudin and B. Gayral, Attribution of the 3.45 eV GaN Nanowires Luminescence to Inversion Domain Boundaries, *Appl. Phys. Lett.*, 2015, **107**, 051904.
56 P. Corfdir, C. Hauswald, J. Zettler, T. Flissikowski, J. Lähnemann, S. Fernández-Garrido, L. Geelhaar, H. Grahn and O. Brandt, Stacking Faults as Quantum Wells in Nanowires: Density of States, Oscillator Strength, and Radiative Efficiency, *Phys. Rev. B: Condens. Matter Mater. Phys.*, 2014, **90**, 195309.
57 G. Jacopin, L. Rigutti, L. Largeau, F. Fortuna, F. Furtmayr, F. Julien, M. Eickhoff and M. Tchernycheva, Optical Properties of Wurtzite/Zinc-Blende Heterostructures in GaN Nanowires, *J. Appl. Phys.*, 2011, **110**, 064313.
58 P. Blanchard, M. Brubaker, T. Harvey, A. Roshko, N. Sanford, J. Weber and K. A. Bertness, Characterization of Sub-Monolayer Contaminants at the Regrowth Interface in GaN Nanowires Grown by Selective-Area Molecular Beam Epitaxy, *Crystals*, 2018, **8**, 178.
59 C. Stampfl and C. G. Van de Walle, Energetics and Electronic Structure of Stacking Faults in AlN, GaN, and InN, *Phys. Rev. B: Condens. Matter Mater. Phys.*, 1998, **57**, R15052.
60 S. Gsell, T. Bauer, J. Goldfuß, M. Schreck and B. Stritzker, A Route to Diamond Wafers by Epitaxial Deposition on Silicon via Iridium/Yttria-Stabilized Zirconia Buffer Layers, *Appl. Phys. Lett.*, 2004, **84**, 4541–4543.